Applied Energy 111 (2013) 161–174

Contents lists available at SciVerse ScienceDirect

Applied Energy

journal homepage: www.elsevier.com/locate/apenergy

Design of a horizontal axis tidal current turbine

Jai N. Goundar, M. Rafiuddin Ahmed *

Division of Mechanical Engineering, The University of the South Pacific, Suva, Fiji

HIGHLIGHTS

- A horizontal axis tidal current turbine is designed for a current speed of 2 m/s.
- Five hydrofoils were designed for the blade from the hub to the tip.
- The characteristics of hydrofoils were studied both experimentally and numerically.
- The 3-bladed 10 m diameter rotor has the maximum efficiency of 47.5%.

ARTICLE INFO

Article history:
Received 20 June 2012
Received in revised form 13 April 2013
Accepted 13 April 2013

Keywords:
Horizontal axis tidal current turbine
Hydrofoils
Cavitation number
Critical coefficient of pressure
Coefficient of power

ABSTRACT

Pacific Island Countries (PICs) have a huge renewable energy potential to meet their energy needs. Limited resources are available on land; however, large amount of ocean energy is available and can be exploited for power generation. PICs have more sea-area than land-area. Tidal current energy is very predictable and large amount of tidal current energy can be extracted using tidal current energy converters. A 10 m diameter, 3-bladed horizontal axis tidal current turbine (HATCT) is designed in this work. Hydrofoils were designed for different blade location; they are named as HF10XX. The hydrodynamic characteristics of the hydrofoils were analyzed. A thick hydrofoil with a maximum thickness of 24% and a maximum camber of 10% was designed for the root region. The maximum thickness of hydrofoils was varied linearly from the root to the tip for easier surface merging. For the tip region, a thinner hydrofoil of maximum thickness 16% and maximum chamber 10% was designed. It was ensured that the designed hydrofoils do not experience cavitation during the expected operating conditions. The characteristics of the HF10XX hydrofoils were compared with other commonly used hydrofoils. The blade chord and twist distributions were optimized using BEM theory. The theoretical power output and the efficiency of the rotor were also obtained. The maximum power at the rated current of 2 m/s is 150 kW and the maximum efficiency is 47.5%. The designed rotor is found to have good efficiency at current speeds of 1–3 m/s. This rotor has better performance than some other rotors designed for HATCT.

1. Introduction

Concerns about the rise in fuel prices and continuous increase in carbon emissions have forced researchers to explore alternative sources of energy [1]. In pacific island countries, imported fossil fuel or petroleum is the primary source for the commercial energy needs. Most isolated islands in pacific use petroleum for transportation and electricity needs. Renewable energy resources are abundant in pacific island countries, and offer a good alternative energy source. The ocean offers a large energy source, for example wave energy, ocean thermal energy, and tidal energy that are yet to be significantly tapped. Tidal current energy is vast, reliable, regular and the most predictable renewable energy resource [2]. Various global studies have shown that tidal current energy has large potential as a predictable sustainable resource for commercial scale generation of electrical power. Tidal current energy is much easier and cheaper to extract using tidal current converters, with less harmful effects to the environmental compared to tidal barrages [3]. Many tidal current energy extraction devices have been developed, but HATCT is the most developed one; it can be used to extract a large amount of tidal current energy from tidal streams. The design and operation of HATCT are similar to those of a Horizontal axis wind turbine (HAWT) [4]. Many developments have taken place in field of HATCT during the recent years, moving from model testing to prototype development and installation. Batten et al. [5,6] made good contribution to the field by designing and model testing of bi-directional marine current turbines. Lee et al. [7] developed a CFD method for power prediction of HATCT. Hwang et al. [8] designed bi-directional horizontal axis tidal turbine (HATT) with improved efficiency by implementing individual blade control. Many turbine with nozzle/duct were developed to

* Corresponding author.
E-mail address: ahmed_r@usp.ac.fj (M.R. Ahmed).

0306-2619/$ - see front matter © 2013 Elsevier Ltd. All rights reserved.
http://dx.doi.org/10.1016/j.apenergy.2013.04.064

Nomenclature

a	axial flow induction factor
a_0	tangential flow induction factor
A	rotor area (m^2)
b	span of hydrofoil in the wind tunnel test section (m)
c	chord (m)
C_D	drag coefficient ($D/0.5\rho bcW^2$)
C_L	lift coefficient ($L/0.5\rho bcW^2$)
C_P	coefficient of pressure ($P_L - P_\infty$)/($0.5\rho bcW^2$)
C_{Pw}	power coefficient = $P/(0.5\rho AW^2)$
D	drag (N)
g	acceleration due to gravity (m/s^2)
h	local head of water at the blade tip immersion $h = h_t + R - r$ (m)
h_t	tip immersion depth (m)
k	Goldstein factor
K_1	wind-tunnel correction constant for solid blockage effects (0.74)
L	lift (N)
M_v	model volume (m^3)
N	number of blades
P	rotor power (W)
P_L	local pressure (N/m^2)
P_∞	freestream static pressure (N/m^2)
P_V	vapor pressure of sea water (N/m^2)
P_{AT}	atmospheric pressure (N/m^2)
Q	rotor tangential force (N)
r	radius of local blade element (m)
R	blade radius (m)
t	thickness (m)
T	rotor thrust (N)
U_0	free-stream velocity (m/s)
V_u	uncorrected free-stream velocity (m/s)
W	relative velocity (m/s) of rotating blade $\sqrt{U_o^2(1-a)^2 + \Omega^2 r^2(1+a')^2}$
X_r	radial distance (r/R)
x	axial coordinate
y	transverse coordinates (m)
α	angle of attack (°)
ρ	density of sea water (kg/ m^3)
ε^{sb}	solid blockage correction factor
Ω	rotational speed (rad/s)
ϕ	angle between W and the plane of rotation (°)
φ	blade pitch angle (°)
σ	cavitation number
σ_k	solidity ratio ($cN/2R$)

Abbreviation

HATCT	horizontal axis tidal current turbines
HAWT	horizontal axis wind turbine
Re	Reynolds number
TKE	turbulence kinetic energy
TSR	tip speed ratio
BEM	blade element momentum
CFD	computational fluid dynamics

improve turbine efficiency – for example the RTT by Lunar Energy [9], SeaGen by Marine Current Turbines (MCTs) [10], some early investigations and testing performed by Thorpe [11] and Clean Current's tidal turbine [12]. However, adding nozzle/duct will increase manufacturing cost as well as weight, the additional manufacturing cost and weight must be justified in terms of increased efficiency. Sale et al. [13] did optimization of HATCT blades using genetic algorithm, which is found to be an effective method for optimizing turbine blades with improved hydrodynamic performance.

For commercial viability of HATCT, a peak tidal current velocity of over 2 m/s is required [5]; a lot of research is being done on HATCT designs, so it can have high efficiency even at lower tidal current velocities. Development and progress in HATCT have made it possible to extract tidal current energy from bi-directional tidal streams by pitching the turbine blade to 180° when the flow reverses [14]. Hydrofoils are individual blade elements that help to convert flow energy into mechanical energy by generating a force and their better design contributes to improved overall performance of the blade. Lift force produced by the hydrofoil rotates the blade as a component of this lift gives the blade its rotating torque. Successful design of blades for HATCT requires one to study the hydrodynamic characteristics of hydrofoils. Hydrofoils work in a similar way as airfoils; however, there are a number of fundamental differences in the design and operation of hydrofoils, which require further investigation, research and development. Particular differences are changes in Reynolds number (Re), different stall characteristics and the possible occurrence of cavitation on hydrofoils. Some useful information is available on the cavitation and stall characteristics of marine propellers (e.g. Ref. [15]), which are very useful for designing of hydrofoils.

Once the cavitation inception is predicted, then the blade element momentum theory (BEM theory) can be applied for predicting the performance of HATCT [13]. BEM theory is widely used for predicting the performance of marine current turbines and the spanwise distribution of blade loading [6]. Another factor that must be taken into account when designing hydrofoils is that water is approximately 830 times denser than air, therefore water exerts larger amount of thrust on marine turbine blades [16]. Thus there is a need to design thicker hydrofoils to meet the strength requirement of the blade to withstand large thrust forces. The designed hydrofoils must have good hydrodynamic characteristics for better performance and delayed cavitation inception.

In the present work, hydrofoils were designed for different sections of a HATCT blade. These sections are for a 3-bladed, 10 m diameter rotor, with an operational tip speed ratio (TSR) of 4 and a free-stream velocity of 2 m/s. The objective was to achieve good hydrodynamic characteristics at tidal current velocities of 1–3 m/s. These hydrofoils were designed to meet certain turbine requirements that are; high performance, good blade strength and non-occurrence of cavitation. All hydrofoils that are designed meet the major requirements of high C_L and high L/D ratio over a wide range of angles of attack. The sections are thick enough to provide strength to the blade and the hydrofoils do not encounter the problem of cavitation at operational TSR of 4 and free-stream velocities up to 3 m/s. Numerical and experimental studies were performed on the HF1020 blade at a location of 60% of the blade from the center of the hub. Initial results were obtained with Xfoil and were verified with both experimental and CFD results.

2. Turbine design parameters and operating conditions

The behavior of hydrofoils is different on a rotating blade compared to when it is not rotating. Once the rotor is in motion, the blade section starts to experience a relative component of tidal current velocity at various angles of attack (α) depending on the blade parameters. The lift and drag forces acting on the hydrofoils

cause the torque and thrust, with the torque producing mechanical power. The direction of tidal current velocity, blade forces and angles are shown in Fig. 1. These components of forces and velocities can be used to predict theoretical rotor performance, using the Blade Element Momentum (BEM) theory. The general BEM theory is based on a combination of momentum and blade element theories. The momentum theory is used to derive the axial and tangential inflow factors with inclusions of tip loss factors to take into account the finite number of rotor blades. The blade element theory is used to model the blade section drag and torque by dividing the rotor blade into a number of elements [6].

Considering momentum, the thrust on an element of the blade due to change in the axial momentum and the torque on an element due to change in the angular momentum, including the Goldstein factor k for finite number of blades will give the equation for thrust (T) and torque (Q) gradients:

$$\frac{dT}{dr} = 4\pi\rho r[U_o^2 a(1-a)k + (a'\Omega rk)^2] \tag{1}$$

$$\frac{dQ}{dr} = 4\pi r^3 \rho U_o \Omega a'(1-a)k \tag{2}$$

Considering the blade elements, the local lift and drag gradient can be defined by:

$$\frac{dL}{dr} = \frac{1}{2}\rho N W^2 C_L \tag{3}$$

$$\frac{dL}{dr} = \frac{1}{2}\rho c N W^2 C_D \tag{4}$$

where N is the number of blades. The rotor thrust and torque can now be defined as:

$$\frac{dT}{dr} = \frac{dL}{dr}\cos\phi + \frac{dD}{dr}\sin\phi \tag{5}$$

$$\frac{dQ}{dr} = r\left[\frac{\mathrm{dL}}{\mathrm{dr}}\sin\phi + \frac{\mathrm{dD}}{\mathrm{dr}}\cos\phi\right] \tag{6}$$

Combining Eqs. 1, 2, 5, and 6 yields equations for axial (a) and tangential (a') inflow factors. These can be solved by iterating ϕ.

$$\frac{a}{1-a} = \frac{\sigma k}{4\pi k X_r \sin^2\phi}\left[C_x - \frac{\sigma_k C_{y^2}}{4\pi X_r \sin^2\phi}\right] \tag{7}$$

$$\frac{a'}{1+a'} = \frac{\sigma_k C_y}{4\pi k X_r \sin\phi\cos\phi} \tag{8}$$

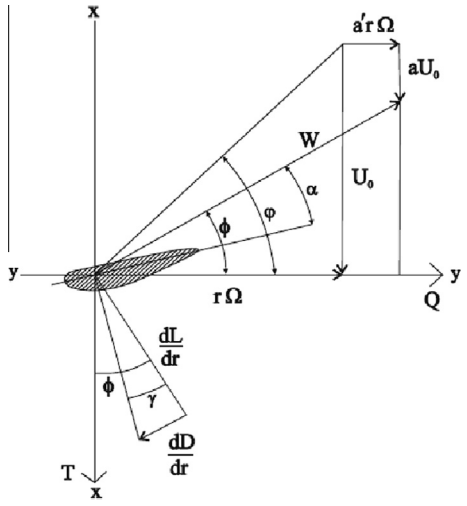

Fig. 1. Velocities and forces on a rotating blade element.

where $C_x = C_L\cos\phi + C_D\sin\phi$, $C_Y = C_L\sin\phi - C_D\cos\phi$, and

The final equations for power and thrust gradients are given by Eqs. (9) and (10), the integration of these equations will give power and thrust.

$$\frac{dC_p}{dx} = \frac{2TSR(1-a)^2\sigma_k X C_Y}{\pi\sin^2\phi} \tag{9}$$

$$\frac{dC_T}{dx} = \frac{2(1-a)^2\sigma_k Cx}{\pi\sin^2\phi} \tag{10}$$

When designing HATCT, the turbine parameters and operating conditions of the turbine must be considered. The basic hydrodynamic design parameters for HATCT include diameter, pitch, twist and chord distribution across the blade span, the stall characteristics, choice or design of blade section and also prediction of occurrence of cavitation at individual blade sections at different operating conditions. The design is further complicated by changing tidal current velocity and direction, shear profile of tidal flow and changing water depths. Most of the design conditions are similar to wind turbines [4], but there are some differences in it's the design and operating conditions – these are, Reynolds number (Re), lower TSR and larger force of water which is about 830 times denser compared to air. The flow speed and TSR are low for HATCTs; the tidal current does not usually exceed 3.5–4 m/s for most of the locations. The TSR of HATCT is between 4.0 and 6.0 [5,6,13,17–19]. Lower TSR is preferable for HATCT to avoid the cavitation inception in turbine blade. The blade loading and performance can be predicted using BEM theory; however cavitation criteria must be predicted at the 2-D design stage. The BEM theory becomes valid for predicting theoretical performance of HATCT rotors once cavitation criteria are determined. Cavitation causes structural damage to the turbine blades and reduces its performance by reducing L/D ratio, the pressures associated with bubble collapse are high enough to cause failure of metal [15]. Therefore a delayed cavitation inception is preferable for HATCT blade sections. Cavitation inception occurs on the blade when the local pressure on the section falls below the vapor pressure of the fluid, and it can be predicted by comparing the minimum suction pressure on the hydrofoil surface with cavitation number σ [5]. The cavitation number is defined as:

$$\sigma = \frac{p_O - p_V}{0.5\rho W^2} = \frac{P_{AT} + \rho gh - p_V}{0.5\rho W^2} \tag{11}$$

In this work, the sea water properties were taken at a salinity of 32 ppt and a temperature of 40 °C, it is assumed that temperature of sea water will not go above 40 °C. Cavitation will occur if the minimum negative pressure coefficient – C_{Pmin} is greater than σ or C_{Pmin} is greater than C_P critical (C_{Pcrit}), C_{Pcrit} is – σ. The chance of cavitation occurring on the blade is greater towards the tip of the turbine blade due to low immersion depth near the tip and the highest relative velocity experienced at the blade tip. For analyzing 2-D section characteristics and predicting cavitation inception, XFoil was used [5]. XFoil is a linear vorticity stream function panel method with viscous boundary layer and wake model, and is found to be suitable for predicting cavitation onset at the preliminary design stage [20].

For predicting cavitation, the C_{Pcrit} at different locations on the blade and tidal current velocities was determined. The C_{Pcrit} at the blade location (r/R) of 0.6 to 1.0 and for tidal current velocities of 2 m/s, 2.5 m/s and 3 m/s are shown in Fig. 2. The C_{Pcrit} for blade tip at tidal current velocities of 1 m/s and 1.5 m/s is around −16 and −8, therefore cavitation cannot occur at these velocities, but once the tidal current velocity increases above 2 m/s, the chance of cavitation increases at r/R of 0.6–1.0. The cavitation may occur for tidal current speed of 2 m/s on the outer 10% of the blade if the minimum C_p drops below −4.0. The minimum C_p should not

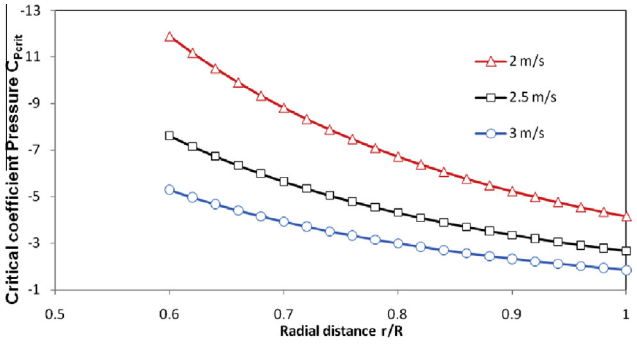

Fig. 2. Variation of the critical pressure coefficient along the blade for different tidal current velocities.

fall below −2.7 for the outer 10% of the blade for the current speed of 2.5 m/s and below – 1.8 for the outer 10% of the blade for the current speed of 3 m/s. For these cases, it is necessary to pitch the blade to avoid cavitation.

The turbine rotor diameter is chosen as 10 m; it has three blades – 3-bladed turbines are more stable and do not cause much vibrations, hence reducing fatigue failures. Also 3-bladed turbines can operate at lower TSR thus reducing chances of cavitation inception [21]. Each blade is 4 m long and the hub with the connection to the blade is 2 m. The rated tidal current speed is 2 m/s, but the turbine is designed to operate in tidal current velocities ranging from 1 m/s to 3 m/s. The operational TSR is chosen as 4. The tidal current assessments are completed at some locations and currently being carried out at some other locations in Fiji's waters at average depths of around 30 m. Last 25% of the total depth from the seabed is left out [22], since the tidal current velocity is lower at the seabed and the flow is highly turbulent. A clearance of 5 m from the sea surface is provided for large waves and for speed boats passing through the passage. Therefore, a turbine diameter of 10–12 m is appropriate for these depths, hence 10 m diameter was chosen.

3. Design of hydrofoils

Hydrodynamic characteristics of hydrofoils that must be studied while designing include the pressure distribution on the hydrofoil's surface, the minimum coefficient of pressure (C_P), coefficient of lift (C_L), coefficient of drag (C_D), and lift to drag ratio (L/D). Some blade parameters that need to be considered when designing hydrofoils are pitch, twist, and taper distribution of the blade and the performance characteristics of a rotating blade. The hydrodynamic design is further complicated due to the non-uniform speed and direction of the current, the shear profile in the tidal flow, and the influence of water depth and the free surface. A challenge faced in designing hydrofoils is to avoid cavitation, while maintaining higher L/D ratio and delayed stall. To make the HATCT perform well under varying conditions, higher C_L and L/D values over a *wide range of* α *are required, with delayed flow separation.* For better efficiency of the HATCT, the C_D should be as low as possible. For structural requirements, blade sections must be thick, especially near the root region. It is important for the turbines to have a section profile such that cavitation inception is delayed. This is achieved when C_P is higher than C_{Pcrit} or $-\sigma$.

The hydrofoils for different blades were designed from existing S1210 airfoil by modifying the maximum camber and maximum thickness; this was done after studying the hydrodynamic characteristics of several airfoils and hydrofoils. The thickness was increased to increase the blade strength and camber was increased to improve the hydrodynamic characteristics of hydrofoils; increasing the camber and maximum thickness for S1210 reduces the minimum suction pressure and increases C_L and L/D ratio. The sections were named as HF10XX series, 10 denotes that hydrofoils have a maximum camber of 10% and XX denotes the thickness of the section at different blade location, which is shown in Table 1. The profile of HF1020 is shown in Fig. 3. Other hydrofoils have similar profiles – only the maximum thickness changes.

A thick hydrofoil was designed for root section which has a maximum thickness of 24% and a maximum camber of 10%; it is named as HF1024. Maximum thicknesses of the hydrofoils were varied linearly from the root to the tip for smooth blade surface merging. For the blade tip a thinner hydrofoil was designed, which has a maximum thickness of 16% and a maximum camber of 10%. This hydrofoil is named as HF1016. Thin section hydrofoils have good hydrodynamic characteristic which is necessary for tip to mid section of the blade. All the hydrofoils have a maximum camber of 10%. The HF1018 has a maximum thickness of 18%, similarly HF1020 and HF1022 have maximum thicknesses of 20% and 22%. This choice of thicknesses ensured good hydrodynamic performance as well as good strength, as the HATCT has to withstand strong hydrodynamic forces.

4. Experimental studies

Model hydrofoil HF1020 was fabricated to test the hydrofoil characteristics by experimentation in the wind tunnel test section. The pressure distribution, lift and drag were determined by experimentation. Pressure taps were provided on the top and bottom surfaces to measure the local pressure on the hydrofoil surface. Fig. 3 shows the pressure tap locations on the surface of the hydrofoil – 18 pressure taps were provided on the top surface and 19 on the bottom surface. The model hydrofoil has a chord length of 100 mm and a span of 300 mm. The hydrofoil was placed in the test section touching both ends of the test section to avoid 3-D flow.

The hydrofoil was tested in an Engineering Laboratory Design (ELD) Inc., low speed open circuit wind tunnel at Re of 190000 (0.19 M) at an air velocity 30.53 m/s; equivalent to a tidal current velocity of 2 m/s, airflows with velocities below 100 m/s are considered incompressible flows; the freestream velocity in this wind tunnel does not exceeds 50 m/s, therefore wind tunnel flow is always considered as incompressible flow. Pressure measurements

Table 1
Hydrofoils designed for different sections of the blade, their maximum thickness and maximum camber.

Turbine section r/R	Hydrofoil	Maximum thickness t/c (%)	Maximum camber (%)
0.2	HF1024	24	10
0.4	HF1022	22	10
0.6	HF1020	20	10
0.8	HF1018	18	10
1	HF1016	16	10

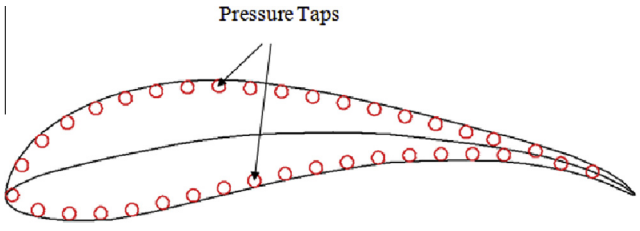

Fig. 3. Hydrofoil HF1020 showing location of pressure taps.

were performed at the angles of attack (α) of 6° and 10°. Placing the airfoil in the test section introduces solid blockage and increases the velocity and hence the Re. The velocity was corrected using Eqs. (12) and (13) [23];

$$V = V_U(1 + \varepsilon^{sb}) \tag{12}$$

$$\varepsilon^{sb} = \frac{k_1(m_v)}{(csa)^{\frac{3}{2}}} \tag{13}$$

where V_u is the uncorrected freestream velocity (m/s), ε^{sb} solid blockage correction factor, K_1 is wind-tunnel correction constant for solid blockage effects (0.74), M_v is model volume (m^3) and *csa* is the cross-sectional area of the wind tunnel test section.

For lift and drag measurements, another model of the HF1020 hydrofoil was fabricated. The hydrofoil has clearance of less than 1 mm from the side walls of the test section to avoid 3-D flow and at the same time ensuring that it does not touch the walls (which will affect the lift and drag measurements). The hydrofoil was mounted on the dynamometer which gives the lift and drag forces acting on the hydrofoil. Lift and drag were measured at Re of 0.19 M which is equivalent to a tidal current velocity of 2 m/s and angles of attack from 0° to 16° at intervals of 2°.

5. Computational fluid dynamic (CFD) analysis

CFD analysis was carried for HF1020 hydrofoil to compare with experimental and XFoil analysis. Hydrofoil geometry was created in Unigraphics (NX4) with the chord length of 100 mm; a thickness of 10 mm was given. The far field was large enough to avoid any blockage, the far field in front of the leading edge, top and bottom surface of the hydrofoil is 12 x chord length and at the back of the trailing edge, it is 20× chord length. The commercial code Ansys-ICEM CFD was used to for mesh generation, To get a higher accuracy, hexahedral grid were generated; very fine meshing was done close to the hydrofoil, for more accurate results. The geometry was imported into Ansys CFX to define boundary condition and solve. ANSY-CFX is a finite volume code used for fluid mechanic analysis. Fluid modeling was used for both meshing and solving.

The inlet water flow velocity was set at 2 m/s for Re 0.19 M and 21.07 m/s for Re 2,000,000 (2 M), velocities were at relative flow angle reference to α for hydrofoil, and working fluid was water at 25 °C. At the outlet, the reference pressure was set to zero, indicating flow is discharged to the atmosphere. Hydrofoil walls were defined as no slip walls and far field walls were defined as no slip walls. Analyses were carried at a freestream turbulence intensity of 1%. For convergence, residual type of RMS and the residual target value of 1×10^{-6} were set as the criteria. The time scale factor was set to 10. The C_D and C_L values were monitored to see if the results converge. The C_P, C_L and C_D values were computed at α between 0° and 16°.

6. Validation of XFoil results with experimental and CFD results

XFoil can be used to predict hydrodynamic characteristics of hydrofoils; however, Xfoil results need to be validated with experimental and numerical (Ansys CFX) results. The XFoil results of C_P distribution and C_L for HF1020 were validated with Experimental and CFD results. Figs. 4 and 5 show the pressure distributions at 6° and 10° α, and at Re of 0.19 M and 2 M. It can be seen that there is good agreement between XFoil, Experimental and Ansys CFX results at Re of 0.19 M for both the α, however, the minimum suction peek predicted by CFD is slightly lower compared to experimental and XFoil results for both the α; at Re of 2 M both XFoil and CFD follow similar trend to that at Re 0.19 M. Thus, there is a good

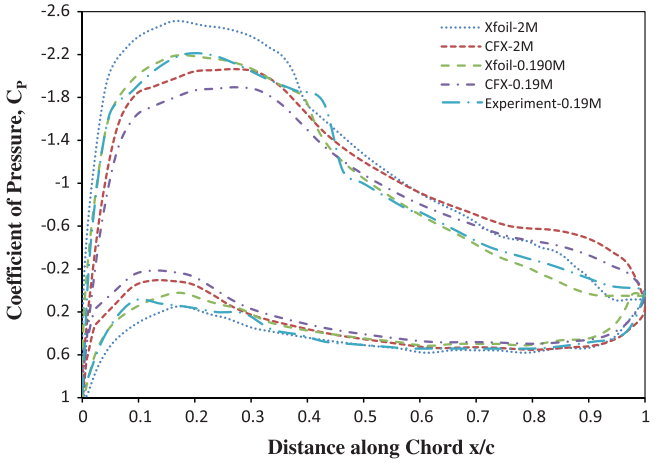

Fig. 4. Pressure distribution on the HF1020 hydrofoil at Re 190,000 and Re 2,000,000 for 6° angle of attack.

agreement between XFOIL and CFD results for the angles of attack of 6° and 10°.

The graphs in Fig. 6 compare the XFoil results of C_L with those from CFD and experimental, for HF1020 at different AOA, and for Re of 0.19 M and 2 M. There is good agreement between XFoil and experimental results at Re 0.19 M, however C_L is slightly underpredicted by CFD. Similar trend is seen for C_L at Re = 2 M.

Both pressure distributions and C_L show good agreement between XFoil, experiments and CFD for Re = 0.19 M and also for Re = 2 M, the graphs at Re = 2 M follow similar trends to those at Re = 0.19 M. Therefore XFoil can be used to predict the hydrodynamic characteristics of hydrofoils at higher Re; Re is always higher for tidal current turbines.

7. Hydrodynamic characteristics for HF10XX hydrofoils

The hydrodynamic characteristics of HF10XX hydrofoil series at Re = 2 M were obtained from XFoil. The average Re is around 2 M along the blade at the rated tidal current speed of 2 m/s and TSR of 4. The most important characteristics that needs to be studied and optimized during the turbine design stage is the C_{Pcrit} for cavitation criteria, C_L and L/D for the efficiency of the turbine. The optimum α needs to be determined, to compare the characteristics of hydrofoils. The optimum α for a hydrofoil can be selected using the drag polar plots. Cavitation criteria also need to be considered while choosing the optimum α, there should not be occurrence of cavitation during the operation of the hydrofoil at the optimum α.

The drag polar plots for the HF10XX hydrofoils are shown in Fig. 7 which were used to choose the optimum α for the HF10XX hydrofoils series. There should be good balance between C_L and C_D, so that the L/D ratio is higher at the optimum α. From the drag polars, the optimum α for HF10XX series hydrofoils is around 12°. The drag polars show increasing C_L with small increase in C_D from 0° to12°, and there is a significant increase in drag after 12° while the lift increases only slightly. Taking into account the variations in the tidal current velocity and direction and also the fact that turbulent flow in the passage can alter the local α of the hydrofoil, the actual optimum α are always few degrees lower than this. Therefore, the optimum operating α for the HF10XX hydrofoils is chosen as 9°.

The plots of C_{Pmin} at different α are important to determine the cavitation criteria of hydrofoils for various operating conditions. The optimum α may be altered if there is cavitation inception at optimum α under operating conditions. For extreme conditions, if the C_{Pmin} is below the C_{Pcrit} at operating α, the blade needs further

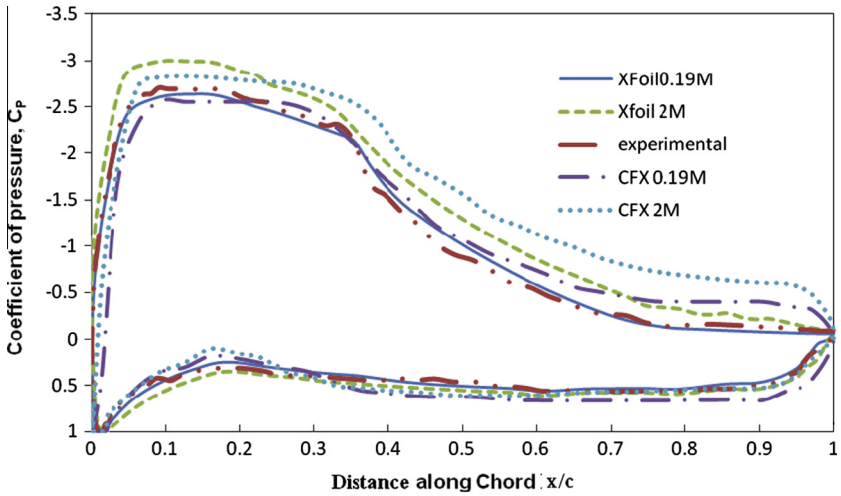

Fig. 5. Pressure distribution on the HF1020 hydrofoil at Re = 190,000 and Re = 2,000,000 for 10° angle of attack.

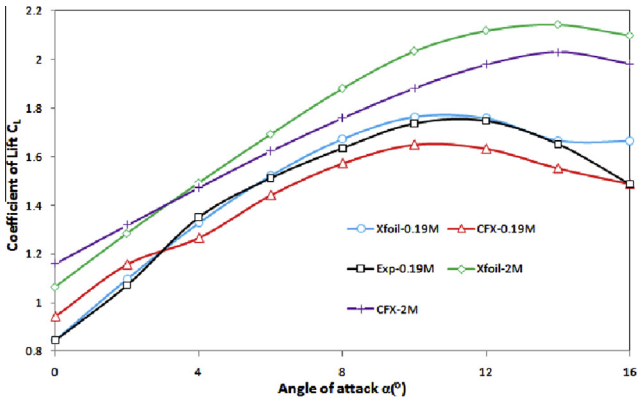

Fig. 6. Variation of the Coefficient of lift for HF1020 with angle of attack at Re = 190,000 and 2,000,000 – comparison of numerical and experimental results.

pitching so the C_{Pmin} increases, and well above C_{Pcrit}. The C_{Pmin} for the HF10XX hydrofoils at Re = 2 M and for different α are shown in Fig. 8. The C_{Pmin} at the operating AOA of 9° is greater than −2.9 for all the blade sections that were designed. Comparing this with C_{Pcrit} from Fig. 2, for tidal current velocities of 2 m/s and below the C_{Pcrit} is below −4.2, this indicates that there will not be cavitation inception on blade sections at tidal current velocities of 2 m/s and below. However, there can be cavitation inception for tidal current velocities above 2 m/s if the local α is 9°, for these cases, the turbine blade needs to be slightly pitched, so that the local α of hydrofoils are below 9° and hence C_{Pmin} is higher to avoid cavitation.

Lift plays a significant role for HATCT, the torque on the rotating blade is obtained from the component of lift force in the tangential direction, and the rotor power is proportional to the torque. It is very complicated to control or determine the component of lift force contributing to the torque for blades operating under changing flow conditions. Therefore, the overall focus is to increase the lift force and reduce the drag force thus maintaining as high an L/D as possible, especially from the mid-section to the blade tip, because this part of the blade contributes towards 70–80% of total power of the rotor. The C_L for the HF10XX hydrofoils at different α and for Re = 2 M are shown in Fig. 9. All the HF10XX series hydrofoils have higher C_L over a wide range of α.

All the HF10XX hydrofoils have high C_L values at the optimum α of 9°; hydrofoils HF1019–HF1016, which are used from r/R = 0.5 to 1, have C_L values of around 2.0 at 9°. The C_L values slightly decrease for hydrofoils near the root – to around 1.8–1.9 for hydrofoils HF1020–HF1023 and to 1.6 for HF1024. The hydrofoils used near the root are thick to provide strength to the blade structure, rather than high efficiency. The maximum strength is required right at the root of the blade, at the blade-to-hub connection, because maximum stress is concentrated at this point. The hydrofoil HF1024 has the maximum thickness of 24%, it is mainly designed to sustain

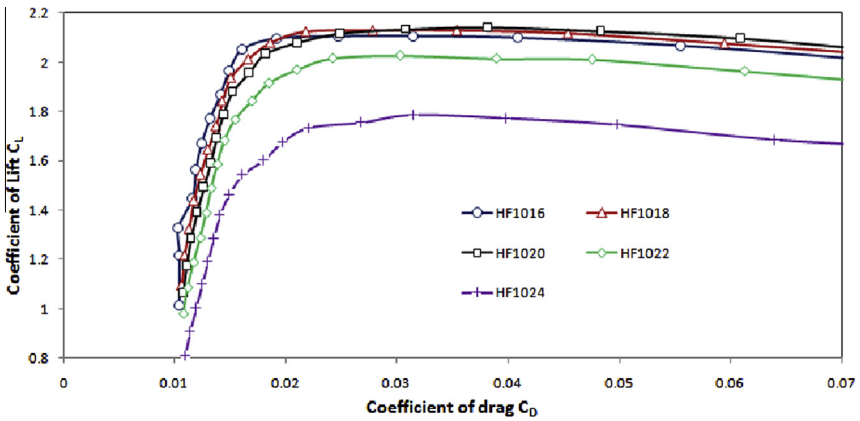

Fig. 7. Drag polars of HF10XX hydrofoil series at Re = 2,000,000.

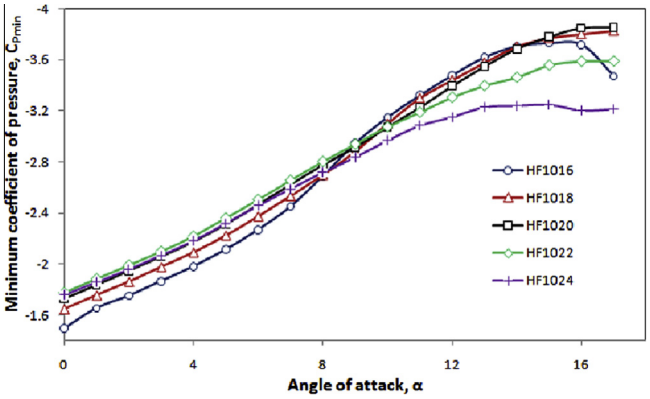

Fig. 8. Minimum coefficient of pressure for HF10XX hydrofoils at Re = 2,000,000.

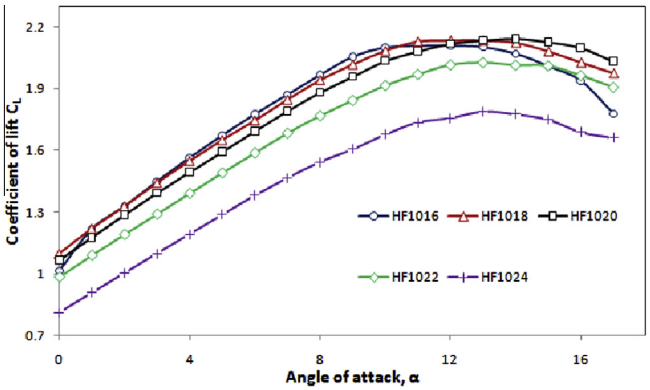

Fig. 9. Variation of the Coefficient of lift for HF1020 hydrofoil with angle of attack at Re = 2,000,000.

the hydrodynamic forces on the blade-to-hub joint. As all the blade sections have high C_L values even at lower α, therefore pitching the blade at tidal current velocities above 2 m/s will still give the rotor good efficiency. The C_L is above 1 for α between 0° and 9° for hydrofoils HF1016–HF1019, around 0.9 for hydrofoils HF1020–HF1023 and around 0.8 for HF1024.

The L/D ratios for all the hydrofoils at different α are shown in Fig. 10. At the operational α of 9°, the L/D is between 100 and 130 for all the hydrofoils except for HF1024 which is around 90. The L/D is higher even at lower α, at α between 1° and 9°, the L/D is around 90–100 for all hydrofoils except for HF1024 for which L/D is around 75. Therefore, these sections can have good performance when the blade is pitched at tidal velocities above 2 m/s to reduce the local α of hydrofoils.

8. Contours of turbulent kinetic energy for HF1020

The contours of turbulent kinetic energy obtained with Ansys-CFX were plotted; these plots show the level of turbulent kinetic energy in the flow over the hydrofoil surface.

The turbulent kinetic energy per unit mass was estimated using the relation

$$T.K.E. = \frac{1}{2}(\overline{u'^2} + \overline{v'^2}) \quad (14)$$

The rise in the turbulence level, the approximate location of transition and the location of flow separation from the surface can be determined from these contours. The flow separates from the upper surface if the flow does not have enough mean kinetic energy to overcome the adverse pressure gradient. If the flow has high mean kinetic energy from the leading edge to the trailing edge, the flow will remain attached till the trailing edge, otherwise the flow will separate.

Flow separation from the upper surface of the hydrofoil adversely affects the blade performance. If the C_{Pmin} decreases too much on the upper surface near the leading edge of hydrofoil, then the flow does not have enough kinetic energy to withstand the adverse pressure gradient downstream and will separate. Early flow separation creates thicker wake region, which results in high pressure drag. The point of flow separation will move away from the trailing edge as α is increased, but if there is early separation at optimum α, then the flow separation can be delayed by shifting the transition point more towards the leading edge. Transition point can be clearly seen in C_P plot, it is denoted by a kink in C_P curve at the upper surface. When the transition point shifts towards the leading edge, the flow separation gets delayed, this reduces the pressure drag, but usually increases the skin friction drag because turbulent flow has a larger skin friction drag [24]. Pressure drag is always greater than skin friction drag at higher α; therefore, shifting the transition point reduces the overall drag, hence, increasing the L/D ratio. The separation point can be determined from the pressure distribution or from the turbulent kinetic energy plot. If the C_P at the upper surface becomes constant (fails to recover after an initial recovery), it indicates flow separation. The separation point can also be seen from the contours of turbulent kinetic energy, at the separation the turbulent kinetic energy in the flow will increase. The contours of turbulent kinetic energy for the HF1020 hydrofoil were obtained using CFX for 6° and 10° at Re of 0.19M and 2M and are shown in Figs. 11–14 to find the locations of transition and flow separation. The separation and transition point can also be seen from the pressure distributions for HF1020 at 6° and 10° at Re = 0.19 M and 2 M, shown in Figs. 4 and 5. From XFoil, the location of transition for the HF1020 airfoil at 6° and Re = 0.19 M is around 0.4c but from the wind tunnel experiments, the location of transition is around 0.42c, and the flow separates at around 0.85c. Experiments show slightly delayed flow separation at about 0.9c. The transition point shifts towards the leading edge when Re is increased for the same α, the transition point shifts to 0.35c, as can be seen from the C_P plots obtained with Xfoil and from experiments at 6° at Re = 2 M. The shifting of transition point results in attached flow till the tralling edge as can be seen in the contours of kinetic energy. Both XFoil and experimental C_P plots show the transition point at 0.35C at the angle of attack of 10° and Re = 0.19 M, and also early flow separation at 0.75c from the Xfoil C_P plots; flow separates at 0.78c from experimental C_P plots and the contours of kinetic energy show flow separating at 0.8c. For Re of 2 M, the transition point shifted to 0.3c from XFoil, and as a result there was attached flow till the trailing edge seen in both the C_P distribution and the contours of turbulent kinetic energy. At higher Re, there is always delayed flow separation, therefore L/D ratio is higher at higher Re. Looking at the L/D values for all the other blade sections, it is clear that all the other sections also have delayed flow sepration.

9. Comparison of hydrodynamic characteristics of HF10XX hydrofoils with other hydrofoils

Commonly used hydrofoils used for HATCT include NACA44XX series, NACA63-8XX series and RisØ-A1-XX series. The hydrodynamic characteristics of HF10XX series hydrofoils were compared with NACA44XX series and NACA63-8XX series.

The comparison of C_{Pmin} for NACA series and HF10XX series is shown in Fig. 15; (see Fig. 16) the optimum α for both the NACA series are around 11°, the optimum α was determined from the

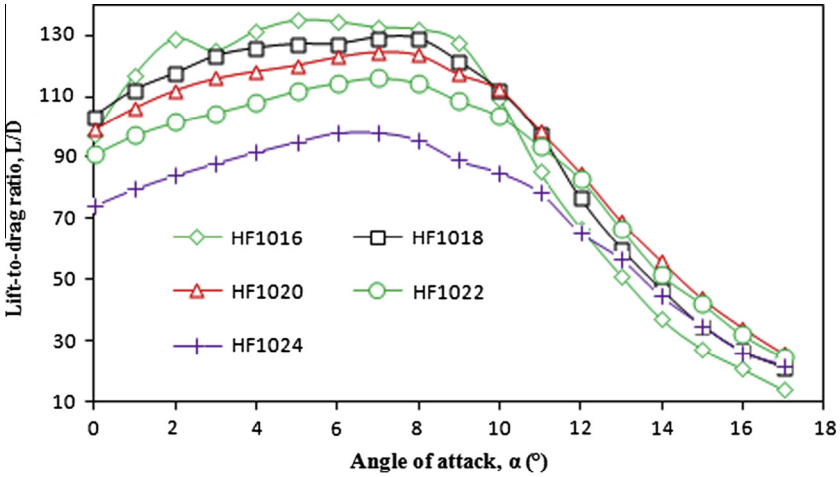

Fig. 10. Variation of the lift-to-drag ratio for HF10XX hydrofoils with angle of attack at Re = 2,000,000.

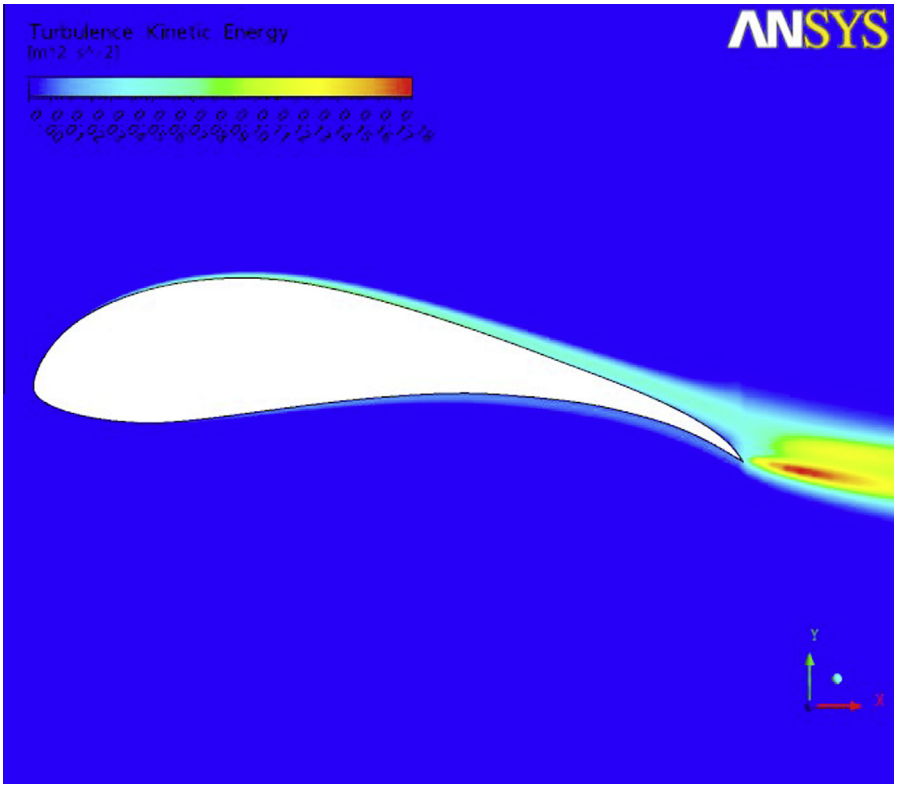

Fig. 11. Turbulent kinetic energy around the HF1020 hydrofoil at $\alpha = 6°$ and Re = 190,000.

drag polars. NACA4415 and NACA4416 hydrofoils are used from the blade tip to the mid-section, C_{Pmin} at the optimum α for these hydrofoils are around −4 and −3.5 respectively at Re = 2 M. NACA 63-812 and NACA63-817 hydrofoils are also used from the tip to the mid-section of 20 m rotor blades, the C_{Pmin} for these sections are −6 and −3.3 respectively at Re = 2 M. The C_{Pmin} of NACA hydrofoils are lower compared to HF1016 and HF1020 which are used from the tip to the mid-section of the blade. Hydrofoils with lower C_{Pmin} are going to experience earlier cavitation even at lower tidal current velocities and will affect the rotor performance in changing tidal flow. Also, C_L was compared at operational α and Re = 2 M, for NACA 44XX series C_L is about 1.5 as shown in Fig. 17 and for NACA 63-8XX series, C_L is between 1.5 and 1.35. The C_L of NACA hydrofoils are lower compared to HF10XX hydrofoils, for which C_L values are between 1.6 and 2. Similarly L/D ratio was compared, L/D for NACA 44XX is around 95 and for NACA 63-8XX, it is between 40 and 50 as shown in Fig. 18, it is lower compared to L/D ratio of hydrofoil HF10XX. Turbine blades with hydrofoils with lower C_L and L/D usually result in lower hydrodynamic performance.

10. Design of rotor

HATCT can be designed if the blades are hydrodynamically optimized for its operating condition, while taking into account the

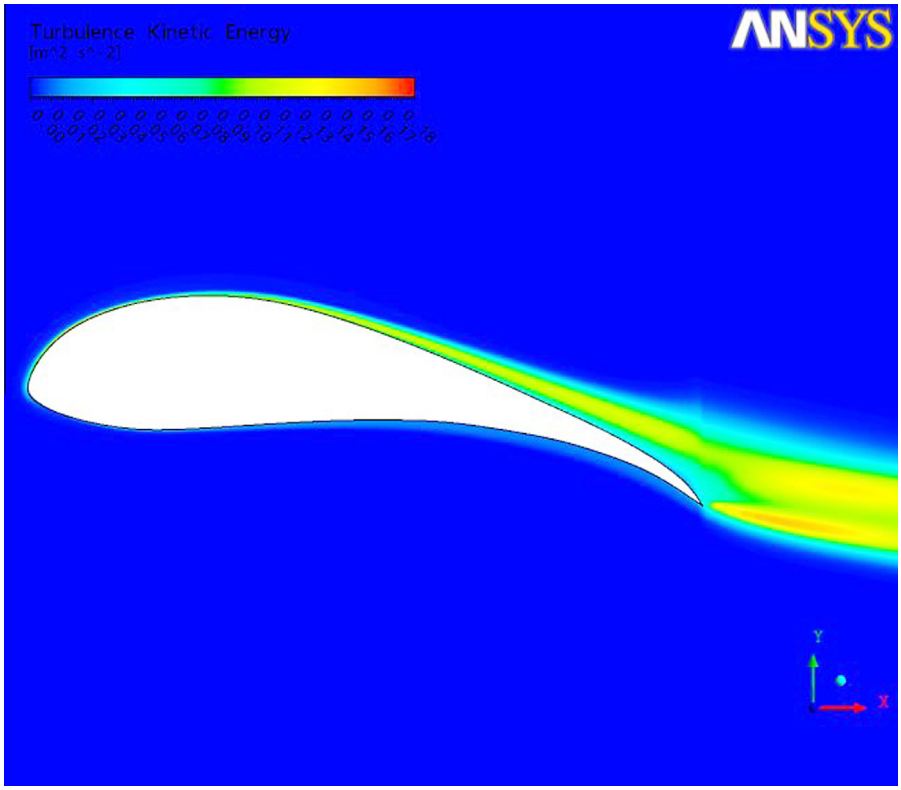

Fig. 12. Turbulent kinetic energy around the HF1020 hydrofoil at $\alpha = 10^{\circ}$ and Re = 190,000.

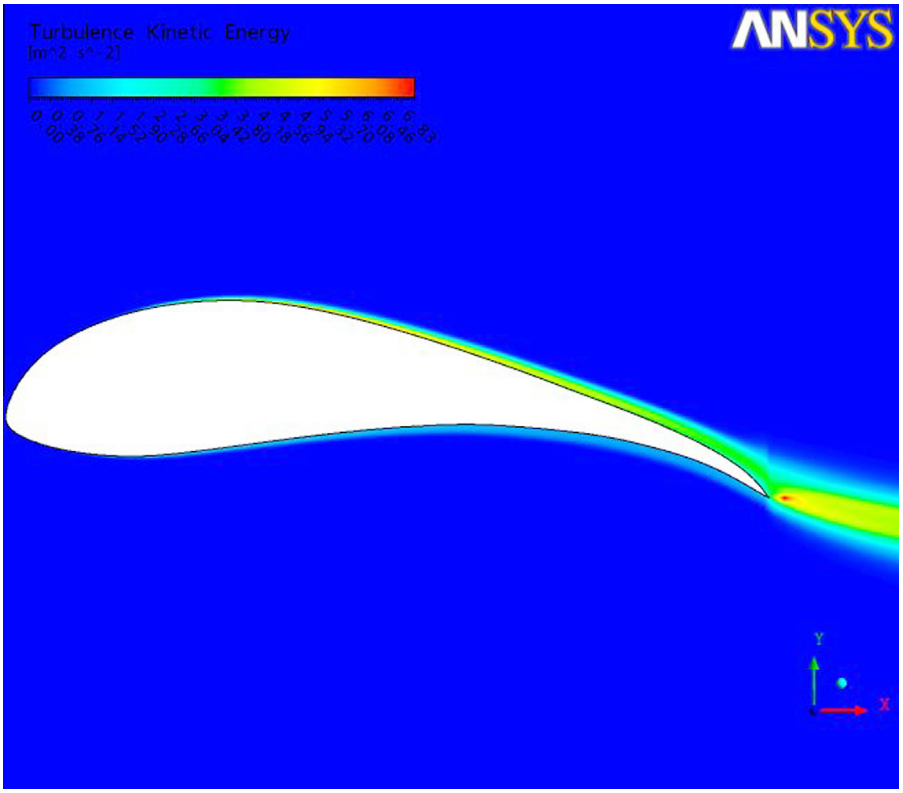

Fig. 13. Turbulent kinetic energy around the HF1020 hydrofoil at $\alpha = 6^{\circ}$ and Re = 2,000,000.

blade cavitation and tip losses. Two major parameters that are required to be optimized are twist distribution and chord distribution. The BEM theory was used to optimize the twist and chord distribution to give the best theoretical performance. Another important component of HATCT is the hub. The hub size frequently used for HATCT is 20% of the rotor diameter, as recommended in

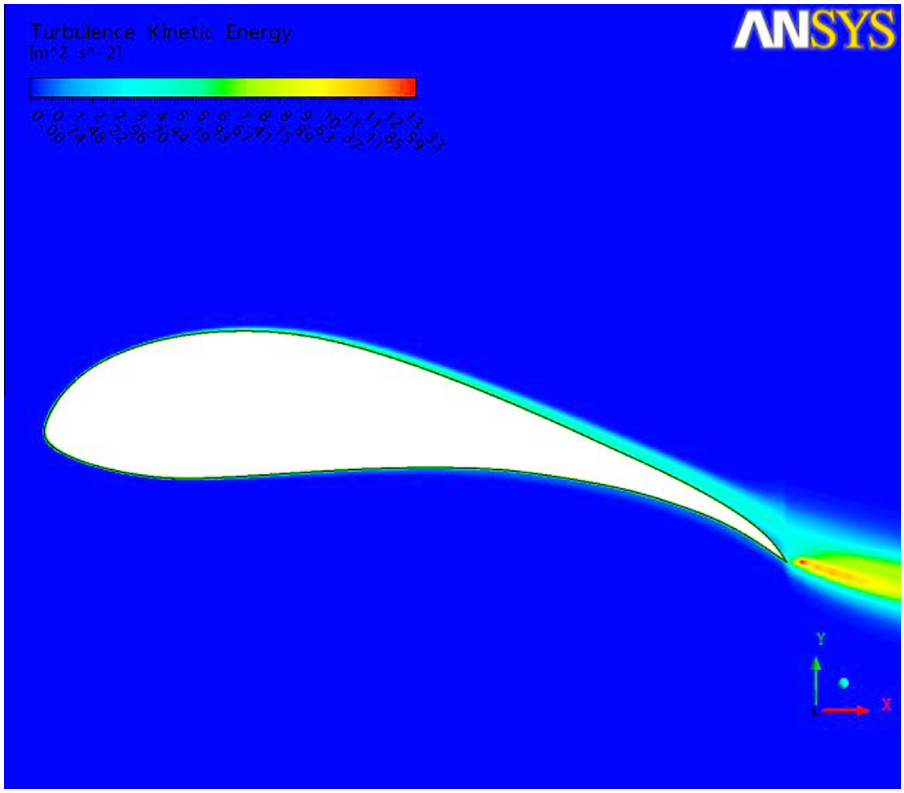

Fig. 14. Turbulent kinetic energy around the HF1020 hydrofoil at $\alpha = 10^{\circ}$ and Re = 2,000,000.

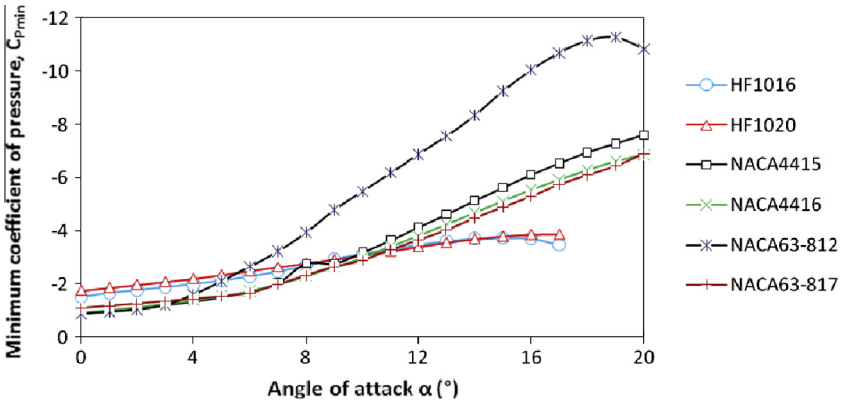

Fig. 15. Comparison of minimum coefficient of pressure for HF1016 and HF1020 with other hydrofoils.

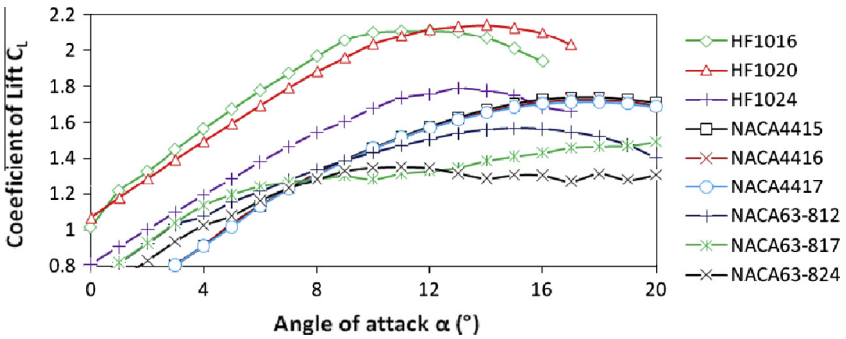

Fig. 16. Comparison of the coefficient of lift for HF10XX with other hydrofoils.

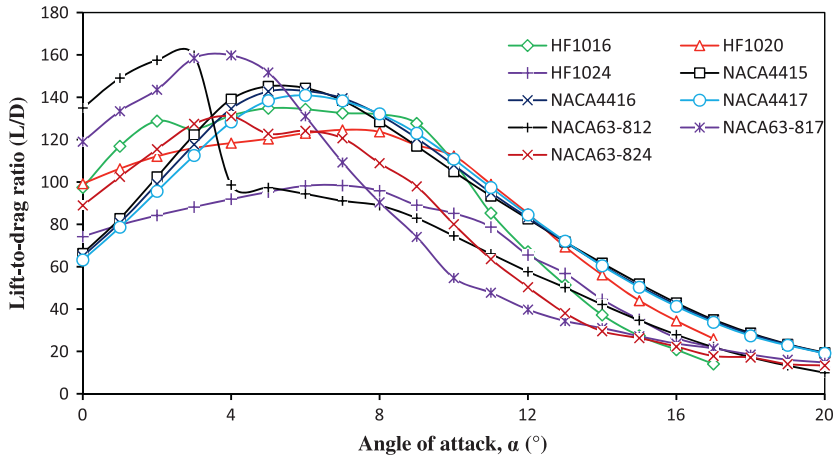

Fig. 17. Comparison of Lift-to-drag ratio for HF10XX with other hydrofoils.

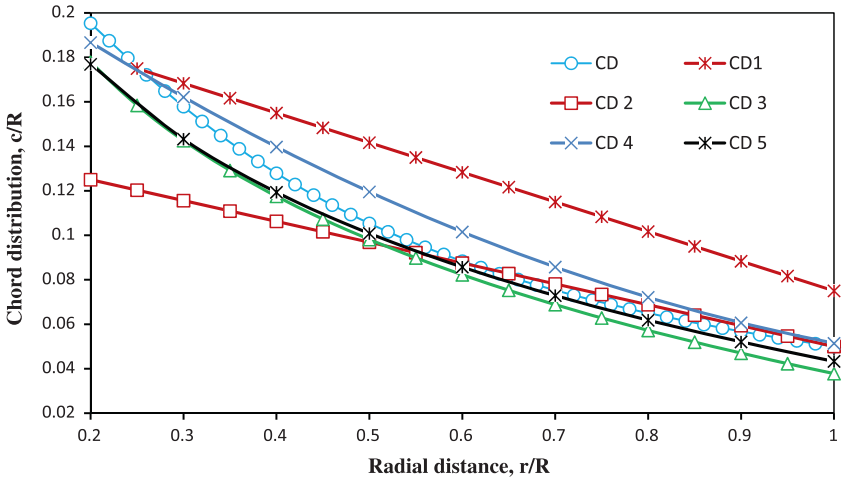

Fig. 18. Chord distributions for various HATCT blades.

Refs. [25,26]. The hub holds the blade rigidly and firmly during rotation, this means that the blade cannot move in flapwise and edgewise directions. There is usually teetering between the hub and the blade to pitch the blade at different angles.

The chord distributions were studied for various HATCT and are shown in Fig. 18. The curves represent the chord distributions: CD1 is the chord distribution that was used for model Contra-Rotating Marine Current Turbine [19], the turbine diameter was 0.81 m and was designed to operate at a TSR of 6. CD2 is the chord distribution that was used for a 20 m HATCT rotor [6], a model 800 mm rotor was designed, manufactured and tested in a towing tank and the model performance was used to predict the performance of the 20 m rotor. Both these turbines used linear chord distribution; a similar linear chord distribution was used by Ju et al. [27] in which a 0.7 m diameter model turbine was constructed and tested in a towing tank. Another model of 11 m rotor having linear chord distribution is presented by Clarke et al. [19]; a 1.5 m model turbine was constructed and tested in a towing tank at a velocity of 2 m/s. Many turbines have linear chord distributions which is preferable from manufacturing point of view. However for better rotor performance, the chord distribution follows hyperbolic curve [28]. The chord distribution curves optimized by a Genetic Algorithm (GA) code for optimized rotor performance are presented by Sale et al. [13]. CD3 shows the chord distribution that was used for Verdant-power's 35 kW Gen4 turbine and was verified with GA code. The same GA code was used to optimize the chord distribution curve for RisØ and NACA hydrofoil rotor, CD4 is the chord distribution for NACA 44XX hydrofoil-based 5 m diameter rotor and CD5 is the chord distribution of the RisØ – A1-XX hydrofoil-based 5 m diameter rotor. A similar chord distribution (but slightly modified) was designed for the present 10 m HATCT with HF10XX hydrofoil blade sections, this chord distribution was then modified taking into account the Re at different sections and variations in the cavitation number, the curve CD represent chord distribution of the blade designed in the present work.

The angle between the plane of rotation and blade (φ) always changes with changing tangential velocity, there is large variation in φ along the blade length, and this makes local α to change along the blade. This problem can be solved by twisting the blade. The blade twist is calculated for one operating condition; minor power losses at other operating conditions cannot be avoided. The twist distribution was optimized for the present blade to yield the best performance under its operating conditions. The optimized twist distribution curve is shown in Fig. 19. Tip vanes are used on HATCT to reduce the tip losses on the blade tips. A "straight trailing edge" [6] was used for the blade tip in the present design, as shown in Fig. 20, solid modeling was done in Auto desk, AutoCAD, AutoCAD is frequently used to model and present mechanical components.

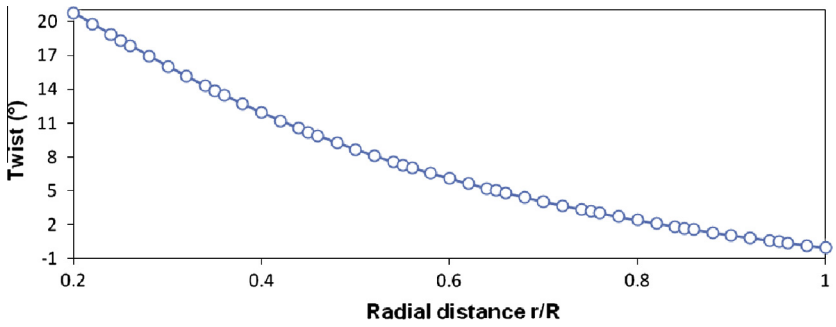

Fig. 19. Optimized twist distribution for the designed blade.

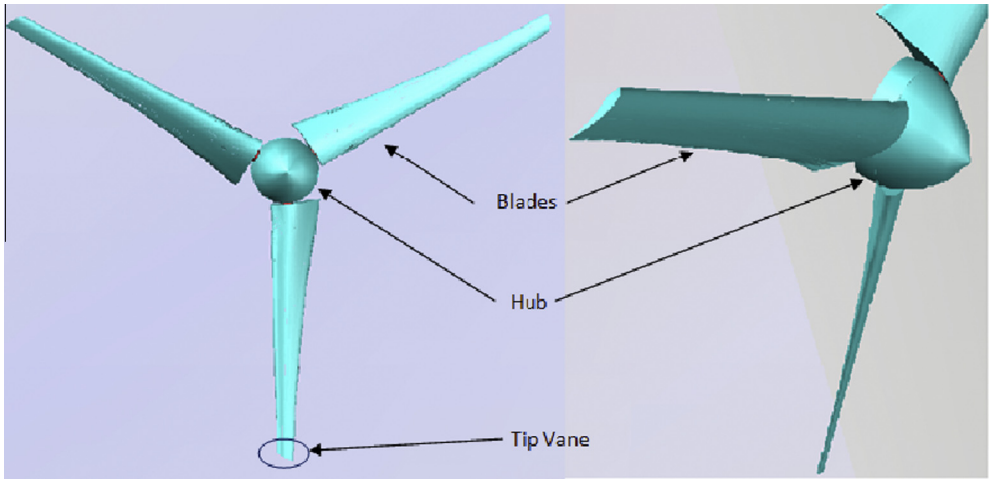

Fig. 20. Geometry of the designed 3-bladed tidal current turbine rotor.

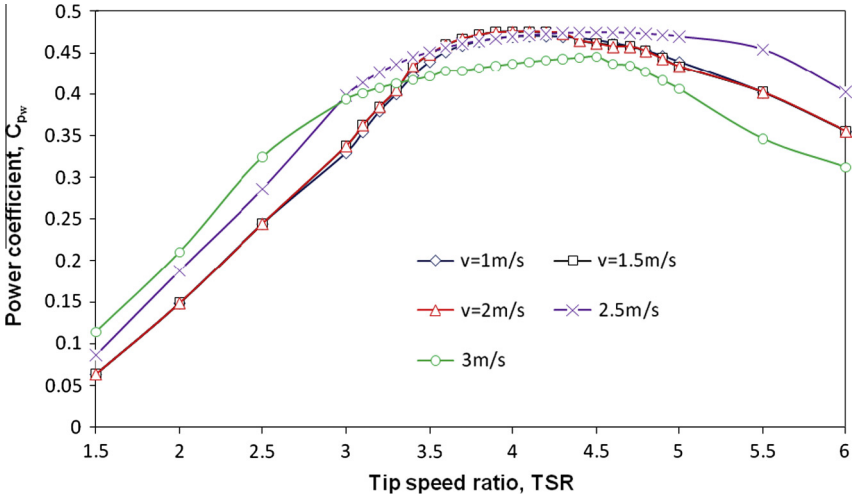

Fig. 21. Coefficient of power for the designed rotor at different tidal current velocities and tip speed ratios.

11. Turbine performance and analysis

The BEM theory is widely used for predicting the theoretical power for rotors at the turbine design stage. It is important to see the rotor performance and optimize the taper and twist distribution for best performance. The theoretical power was predicted using BEM theory and was validated using experimental results [6]. There is very good agreement between experimental and theoretical power prediction and validates the BEM theory, and it can be used to predict the power for HATCT at the design stage. The BEM theory predicts the rotor performance analyzing and matching the blade forces generated by the blade element to the momentum changes occurring in the fluid through the rotor disk.

For the 10 m HATCT rotor designed for the rated tidal current velocity of 2 m/s and TSR of 4, the rotor power and efficiency (C_{Pw}) at different TSR and tidal current velocities were calculated

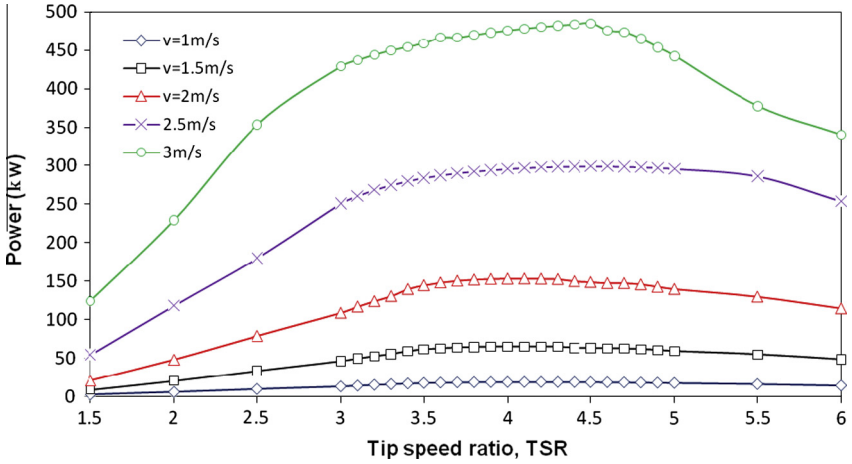

Fig. 22. Power output for the designed rotor at different tidal current velocities and tip speed ratios.

using BEM theory and the results are shown in Figs. 21 and 22. Table 2 shows the local α of blades sections at different tidal current velocities and at the TSR of 4. The blade was pitched to 20.75° (the pitch angle is between plane of rotation to the chord line of hydrofoil at the blade root), for tidal current speeds of 1 m/s, 1.5 m/s and 2 m/s the pitch is actually equal to the maximum twist at blade root. But the blade was further pitched to 24.75° for the current speed of 2.5 m/s so there is good margin between C_{Pmin} at the blade's local α and C_{Pcrit}. Similarly, the blade needs to be pitched to 28.75° for tidal current velocity of 3 m/s so there is no cavitation inception in extreme conditions.

The maximum theoretical power at the rated tidal current velocity of 2 m/s and TSR of 4 is 150 kW. About 75% of total power is produced from mid section to the tip of the blade that is from r/R of 0.5 to 1; there this part is hydrodynamically optimized for better efficiency. The blade from midway to the root does not contribute much towards mechanical power; therefore, this part is mainly thick to provide strength to the blade. The maximum efficiency of the rotor at 2 m/s and at TSR of 4 was 47.6%. The rotor has higher C_{Pw} over a wide range of TSR, C_{Pw} is around 0.47 for TSR of 3.3–4.7, the TSR can fluctuate in actual operating conditions due to turbulence in the incoming flow. Therefore, the turbine must maintain its efficiency at other TSR. This turbine has higher efficiency over a wide range of TSR, therefore, it will perform well in changing conditions. The local α at TSR of 4 and Tidal current velocity of 2 m/s is between 7.7 and 9.2, that is between optimum operational α, giving the maximum C_L of around 1.9. For these AOA, C_{Pmin} is around −2.6 from Fig. 8 that is way above C_{Pcrit} which is −4.7 from Fig. 2. Therefore, there will not be any cavitation at the rated tidal current speed of 2 m/s and TSR of 4.

Table 2
Local angle of attack of hydrofoils at different locations on the blade from the root to the tip for different tidal current speeds at the TSR of 4.

r/R	1 m/s	1.5 m/s	2 m/s	2.5 m/s	3 m/s
	α				
0.25	7.748	7.8305	7.918	8.539	6.359
0.3	7.662	7.7365	7.824	7.373	5.183
0.35	7.59	7.7075	7.795	7.068	4.764
0.4	7.688	7.8445	7.932	6.449	4.104
0.45	7.75	7.9095	7.997	6.348	3.887
0.5	7.972	8.1295	8.217	6.036	3.512
0.55	8.077	8.2435	8.331	6.023	3.399
0.6	8.335	8.5125	8.6	5.892	3.182
0.65	8.429	8.6035	8.691	5.893	3.102
0.7	8.703	8.8775	8.965	5.895	3.032
0.75	8.743	8.9085	8.996	5.866	2.942
0.8	8.956	9.1025	9.19	5.626	2.706
0.85	8.847	8.9715	9.059	5.487	2.531
0.9	8.853	8.9595	9.047	5.167	2.203
0.95	8.514	8.5915	8.679	4.445	1.576

At the cut-in tidal current speed of 1 m/s, the maximum power output is around 19 kW, and maximum C_{Pw} of 0.47 at TSR of 4. The maximum power and C_{Pw} increased to 64.6 kW and 0.475 for tidal current speed of 1.5 at TSR of 4 for both the velocities of 1 m/s and 1.5 m/s, the local α of blade was between 7.7° and 9° that is in range of optimum α for all the blade section. There is no cavitation inception at tidal current velocities of 1 m/s and 1.5 m/s. At 2.5 m/s, the maximum power output is around 290 kW and maximum C_{Pw} is 0.471 at TSR of 4. The local angles of attack of hydrofoils were slightly lower between 4.5° at the tip and 8.5° at the root, this is because blade was pitched extra to increase the local C_{Pcrit}, hence reducing chance of cavitation; especially towards the tip of the blade, the local α is 4.5° for which C_{Pmin} is around −2; it is above the C_{Pcrit} which is around −3 from Fig. 2. The turbine was designed to operate at extreme sea conditions at maximum or cutoff tidal current speed of 3 m/s. At 3 m/s and TSR of 4, the maximum power achieved is around 475 kW at the efficiency is 44%, the efficiency decreases because of pitching of blade at a lower angle. The extra pitching of the blade reduces the local α at the tip, it is 1.3° for which the minimum C_P is −1.7 it is above the C_{Pcrit} which is −2.1. The tidal current speed is not generally predicted to exceed 3 m/s for Fiji. However the turbine is designed to operate at cut-off tidal current speed of 3.5 m/s in unpredictable extreme sea conditions.

The designed rotor has better theoretical efficiency than some of the HATCT rotors presented; which are, a 3-bladed 20 m diameter rotor designed and presented in reference [26] having the maximum efficiency of 45% at rated tidal current speed of 2 m/s, another three bladed 20 m rotor designed and presented in reference [6] has the maximum theoretical efficiency of 45% operating at rated tidal current speed of 2 m/s and TSR of 4. The present rotor has an efficiency similar to the 3-bladed; 5 m rotor designed and optimized using genetic algorithm which is presented in reference [13], it has maximum efficiency around 47–48% operating at rated tidal current velocity of 2.1 m/s. The present rotor has achieved good performance; the hydrofoils were carefully designed to have good hydrodynamic characteristics and the chord distribution and twist distribution were optimized to maximize the rotor performance.

The technology of HATCT is still developing, further research and deployment needs to be done, before this technology can be of direct commercial use; developments are needed particularly in the area of materials; it can help solve the problem of cavitation,

and that of blade strength. Materials which prevent erosion of blades from cavitation can help prolong the life of the blades and improved their performance. Bio-fouling of the blades is also a major problem of HATCT, blade fouling significantly affects rotor performance, especially when it is operating at higher TSR. Special application of coating on blades to prevent and regular maintenance is required.

12. Conclusions

A horizontal axis tidal current turbine is designed for a current speed of 2 m/s. The 3-bladed turbine has a diameter of 10 m. Hydrofoils were designed for different locations along the radial distance with the objective of maximizing the lift-to-drag ratio and avoiding cavitation. The thicknesses of the sections varied from 16% close to the tip to 24% close to the root; this ensured good hydrodynamic performance as well as good strength, as the HATCT has to withstand strong hydrodynamic forces. All the sections designed showed good hydrodynamic characteristics, which are required in a high performance turbine – it was ensured that the coefficient of lift does not drop significantly even if the angle of attack varies from the design angle. The hydrofoil characteristics obtained with Xfoil were verified with experimental and CFD results. The rotor has a maximum efficiency of 47.6% at the rated tidal current speed of 2 m/s and TSR of 4; it performs better than some of the rotors already designed, due to special focus on the design of hydrofoils and the optimum chord and twist distributions used. The rotor performance does not deteriorate even if the current speed changes or if the TSR changes from the design values. In future work, CFD of full model of HATCT can be done at different turbulence intensities and free-stream velocities to evaluate the turbine performance at varying turbine operating conditions.

References

[1] Charlier RH. A " Sleeper" awakes: tidal current power. Renew. Sustain. Energy Rev. 2003;7(3):187–213.
[2] Pontaa FL, Jacovkis PM. Marine-current power generation by diffuser-augmented floating hydro- turbines. Renew Energy 2007;33:665–73.
[3] Rourke FO, Boyle F, Reynolds A. Tidal energy update 2009. Ireland: Department of Mechanical Engineering; 2009.
[4] Burton T, Sharpe D, Jenkins N, Bossanyi E. Wind energy handbook. Wiley; 2000.
[5] Batten WMJ, Bahaj AS, Molland AF, Chaplin JR. Hydrodynamics of marine current turbine. Renew Energy 2006;31:249–56.
[6] Batten WMJ, Bahaj AS, Molland AF, Chaplin JR. The prediction of Hydrodynamic performance of marine current turbines. Renew Energy 2006;33:1085–96.
[7] Lee JH, Park S, Kim DH, Rhee SH. Kim MC Computational methods for performance analysis of horizontal axis tidal stream turbines. Appl Energy 2012;98:512–23.
[8] Hwang IS, Lee YH, Kim SJ. Optimization of cycloidal water turbine and the performance improvement by individual blade control. Appl Energy 2009;86:1532–40.
[9] Jones JA, Chao Y. Offshore hydrokinetic energy conversion for onshore power generation. In: ASME 2009 28th international conference on ocean, offshore and arctic engineering (OMAE2009), Honolulu, Hawaii, May 31–June 5, 2009.
[10] Fraenkel P. Development and testing of marine current turbine's SeaGen 1.2MW tidal stream turbine. In: International conference on ocean energy, ICOE 2010, Bilbao, Spain, October 2010.
[11] Thorpe T. The advantages of ducted over unducted turbines. In: 6th European wave and tidal energy conference; 2005. p. 523–8.
[12] Niet T, McLean G. Race rocks sustainable energy development. In: 11th Canadian hydrographic conference, Victoria, British Columbia, June 2001.
[13] Sale D, Jolman J, Musial W. Hydrodynamic optimization method and design code for stall- regulated hydrokinetic turbine rotor. National Renewable Energy Laboratory; 2009.
[14] Peter P, Fraenkel P. Marine current turbines: an emerging technology, Scottish hydraulics study group seminar, renewable energy, 2004.
[15] Carlton JS. Marine propellers and propultion. Butterwworth Heinemann; 1994.
[16] Bryden IG, Grinsted T, Melville GT. Assessing the potential of a simple tidal channel to deliver useful energy. Appl Ocean Res 2004;26(5):198–204.
[17] Molland AF, Bahaj AS, Chaplin JR, Batten WMJ. Measurements and prediction of forces, pressure and cavitation on 2-D sections suitable for marine current turbines. J Eng Maritime Environ 2004;218:127–38.
[18] Coiro DP, Maisto U, Scherillo F, Melone S, Grasso F. Horizontal axis tidal current turbine: numerical and experimental investigations. University of Naples, Department of Aeronautical Engineering (DPA); 2006.
[19] Clarke JA, Connor G, Grant AD, Johnstone C, Ordonez-Sanchez S. A contra-rotating marine current turbine on a flexible mooring: Development of a scaled prototype. In: 2nd International conference on ocean energy, Brest, France; 2008.
[20] Drela M. XFoil: an analysis and design system for low Reynolds number airfoils. Conference on low Reynolds number airfoil aerodynamics. University of Notre Dame; 1989.
[21] Goundar JN, Ahmed MR, Lee YH. Numerical and experimental studies on hydrofoils for marine current turbines. Renew Energy 2012;42:173–9.
[22] Bryden IG, Naik S, Fraenkel P, Bullen CR. Matching tidal current plants to local flow conditions. Energy 1988;23(19):699–709.
[23] Barlow JB, Rae WH, Pope A. Low speed wind tunnel testing. 3rd ed. New York: John Wiley and Sons; 1999.
[24] Ahmed MR. Blade sections for wind turbine and tidal current turbine applications – current status and future challenges. Int J Energy Res 2012;36:829–44.
[25] Nicholls-Lee RF, Turnock SR. Enhancing performance of a horizontal axis tidal turbine using adaptive blades, IEEE conference. Southampton: University of Southampton; 2007.
[26] Nicholls-Lee RF, Turnock SR, Boyd SW. Simulation based optimisation of marine current turbine blades. In: 7th international conference on computer and IT applications in the maritime industries. Belgium: Liège; 2008.
[27] Ju HL, Dong HK, Shin HR, In RD, Byung CS, Moon CK. Computational and experimental analysis for horizontal axis marine current turbine design. Hamburg, Germany: Second International Symposium on Marine Propulsors; 2011.
[28] Hau E. Wind turbines. Berlin Heidelberg: Springer; 2006.